Balancing free-volume and hydrogen-bond/ion-pair interactions: Plasticisation of cassava starch with glycerol-monoethanolamine deep eutectic solvents

Chien Van Nguyen, Mai Thi Pham, Phuong Thi Hoang*

Institute of Chemistry, Vietnam Academy of Science and Technology

18 Hoang Quoc Viet, Nghia Do Ward, Hanoi, Vietnam

Received 26 September 2025; revised 14 October 2025; accepted 6 November 2025

Abstract

Thermoplastic cassava starch was plasticised with deep eutectic solvents (DES) based on choline chloride (ChCl), glycerol (Gly), and monoethanolamine (MEA) to balance free-volume creation and hydrogen-bond/ion-pair junctions. Binary (ChCl:Gly 1:3; ChCl:MEA 1:3) and ternary ChCl:Gly:MEA (1:1:1; 1:1:2; 1:2:1) DES at 25 wt% were melt-compounded and assessed by processing metrics, FTIR-ATR, Dynamic Mechanical Analysis (DMA), Scanning electron microscopy (SEM), X-ray diffractometry (XRD), wettability (Owens-Wendt-Rabel-Kaelble (OWRK)), and 56-day ambient aging (23±2°C, 50±5% RH). Gly-rich systems enhanced flow but depressed cohesion, whereas MEA-rich systems strengthened interchain junctions. The ternary ChCl:Gly:MEA 1:1:2 delivered the best process-structure-property balance, combining high melt processability with TS≈2.9 MPa and ε_b≈195% (n=5) and displaying the lowest 56-day ductility loss ($\Delta\varepsilon_b$≈-17%) compared with glycerol controls (≈-50%). FTIR (O-H/N-H red-shift and broadening), together with SEM fracture morphology and OWRK-derived surface energetics, supports a dual-mode plasticisation mechanism in which MEA-enabled junctions counterbalance Gly-induced free volume, thereby stabilising the amorphous phase and retarding retrogradation without sacrificing strength. This composition-structure map identifies ChCl:Gly:MEA (1:1:2) as a composition window that stabilises TPS mechanical performance during ambient aging.

Keywords: **deep eutectic solvents, dual-mode plasticisation, monoethanolamine, retrogradation, thermoplastic starch.**

Classification number: **2.2**

*Corresponding author: Email: hoangphuong15@gmail.com

1. Introduction

Starch-based thermoplastics (TPS) are compelling candidates for sustainable packaging and agricultural uses because starch is abundant, renewable, low-cost, and biodegradable [1, 2]. However, native starch is brittle and difficult to process: its semicrystalline framework, stabilised by dense intra- and intermolecular hydrogen bonding between amylose and amylopectin, limits chain mobility, elevates Tg, and narrows the melt-processing window [3]. Plasticisation is therefore required to disrupt this network and enable thermoplastic flow. Conventional plasticisers (glycerol, sorbitol, urea) can improve flexibility; among them, glycerol is prevalent owing to availability and price [4]. Yet glycerol-plasticised TPS commonly exhibits excessive moisture uptake, strong retrogradation, and loss of tensile strength during storage - consequences of a free-volume-dominated mechanism that depresses T_g but weakens cohesive interactions [2, 3, 5]. Binary/ternary mixtures (e.g., glycerol-sorbitol, glycerol-urea) partially mitigate these trade-offs by combining complementary interactions [6, 7].

Deep eutectic solvents (DES) have recently emerged as tuneable, cost-effective "designer" plasticisers for polysaccharides [8]. DES are formed by pairing a hydrogen-bond acceptor (HBA; e.g., choline chloride) with hydrogen-bond donors (HBDs; polyols, amides, or amines), producing eutectic systems with depressed melting points yet strong polarity and H-bonding capacity. Prior studies show that DES such as ChCl:urea and ChCl:glycerol can plasticise starch, reduce crystallinity, and increase extensibility; DES have also been explored in TPS-lignin systems [9], improving interfacial interactions and processability under melt conditions. Despite this progress, component-level roles remain under-resolved. Polyols (e.g., glycerol) primarily generate free volume, strongly lowering T_g but compromising strength, whereas amines such as monoethanolamine (MEA) can act as both HBD and (to a degree) HBA, forming H-bond/ion-pair junctions with choline chloride and starch hydroxyls that may temper T_g depression and recover load bearing [8, 10]. Systematic, side-by-side comparisons of glycerol-rich, MEA-rich, and ternary glycerol–MEA DES at fixed content and identical processing are scarce. Moreover, quantitative links among spectroscopic H-bond signatures (FTIR), rheology (torque, MFI), morphology (SEM), and macroscopic properties (TS, ε_b, T_g) remain limited.

Here we address these gaps by fixing DES at 25 wt% and implementing standardised compounding (internal mixing, twin-screw extrusion, hot pressing) to

compare ChCl:Gly, ChCl:MEA, and ChCl:Gly:MEA ternaries across controlled compositions. We test the hypothesis that glycerol-rich DES maximise extensibility but reduce strength (free-volume dominance), MEA-rich DES partially recover strength via reversible –OH/–NH H-bond/ion-pair junctions, and ternary formulations provide a balanced window of ductility, strength, and processability. By integrating FTIR, DMA, mixing/MFI/SME, SEM, and tensile metrics, we establish a composition–structure–property map that clarifies how DES chemistry governs mobility versus supramolecular association in TPS. The resulting guidelines support rational selection of multifunctional, sustainable plasticisers for next-generation starch-based bioplastics.

2. Experimental Section

2.1. Chemicals

Cassava starch (CS) with an amylose content of 22–28 %, a moisture content of approximately 13 %, and an ash content of 0.2 % was obtained from NEO Nam Vietnam Co., Ltd. Glycerol (Gly) (≥99.5 % purity) was purchased from Sigma-Aldrich and used as received. Monoethanolamine (MEA, Sigma-Aldrich), glycerol and deep eutectic solvents (DES) were used as plasticisers in this investigation. To make the DESs, choline chloride (ChCl), glycerol and MEA were mixed together in respective molar ratios of 1:3:0, 1:0:3, 1:1:1, 1:2:1, 1:1:2 and then heated to 80-90°C until the combination turned into a clear, smooth liquid; then, the mixture was sealed and stored at ambient condition.

2.2. Preparation of thermoplastic starch (TPS) samples

Thermoplastic starch (TPS) samples prepared via twin-screw melt compounding (HAAKE Rheomex PTW16/25 OS, Thermo Scientific, Germany) located at the Institute of Chemistry. Cassava starch powder was dried at 60 ^{o}C for 8 h before quantification and fed into the extruder by a feeder. The plasticisers (DES) with specified content (Tab. 1), fed into the extruder by a liquid feeder pump. Synthetic mixing is carried out at the following temperatures of the mixing zones: feeder zone: 110^{o}C, melt zone: 120-125^{o}C, mixing and conveying: 115-120^{o}C, die temperature: 110^{o}C, and at a screw speed of 150 rpm. The extruded samples were cooled to room temperature and then dried for 24 h after pelletising. The TPS-DES samples obtained were then moulded into sheets of 3.00 mm in thickness by hot pressing at 120°C for 2 minutes with a pressure of 20 tons, followed by cooling to room temperature. The sheets were used for further characterisation.

Table 1. Formulation of TPS samples with varying DES.

Samples	**Composition (g)**		**Plasticiser type**	**DES** ***Ratio***		
	Cassava starch	***Plasticiser***		*ChCl*	*Glycerol*	*MEA*
TPS-Gly	75	25	Glycerol	-	-	-
C.G: 1:3	75	25	DES	1	3	-
C.M: 1:3	75	25	DES	1	-	3
C.G.M: 1:1:1	75	25	DES	1	1	1
C.G.M: 1:1:2	75	25	DES	1	1	2
C.G.M: 1:2:1	75	25	DES	1	2	1

Note: DES: deep eutectic solvent, G and Gly: glycerol, M: Monoethanolamine, C: choline chloride.

2.3. Analytical methods

2.3.1. Processing rheology: Compounding behaviour was monitored on a HAAKE Rheomex 600 closed mixer (Haake, Germany) at 120°C, 100 rpm, for 10 min. Torque-time and stock temperature-time traces were recorded (PolySoft OS). The steady-state torque was calculated as the average over the final 3 min. Specific mechanical energy (SME) was obtained by integrating the torque-time curve multiplied by angular speed and normalising by sample mass (n=3) and is displayed in the energy-time plots.

2.3.2. Tensile properties: Compression-moulded plaques were die-cut into ASTM D638 Type IV dumbbell specimens (gauge length 25 mm; neck width 6.00±0.05 mm; thickness 3.00±0.10 mm). Tests were performed on a 10 kN universal testing machine at a crosshead speed of 20 mm/min at ambient conditions. Tensile strength (TS) and elongation at break (ε_b) were extracted from engineering stress-strain curves, following ASTM D638 using an AGX-V Testing Machine (Japan). Values were averaged over five specimens (n=5).

2.3.3 Dynamic Mechanical Analysis: Rectangular strips were tested in single-cantilever mode at 1 Hz with a strain amplitude of 0.1 %, which lies within the linear viscoelastic regime (LVR) as verified by preliminary strain-sweep checks on representative samples (no time-dependent drift of E′ during isothermal holds). Specimens were pre-conditioned at 23±2°C and 50±5% RH for at least 48 h, sealed prior to testing, and scanned under dry N_2 purge. Thermal scans were run from -40 to +120°C at 10°C/min under dry

N_2 purge. Because the materials are plasticised systems, data interpretation is restricted to the low-temperature window around the primary glass transition (T_g) where plasticiser mobility dominates; the upper part of the scan is reported for completeness but is not used to infer plasticiser-controlled behaviour. Reported T_g corresponds to the tan δ peak temperature (±SD, n=3), and E′ values were taken at the indicated temperatures after baseline stabilisation.

2.3.4. FTIR-ATR Spectroscopy: Spectra were recorded on a NicoletTM iS50 (ATR mode, diamond) over 4000-500 cm^{-1} with 4 cm^{-1} resolutions and 16 scans per spectrum.

2.3.5. Morphology: Scanning electron microscopy (SEM, SM-6510LV (JEOL, Japan) at the Institute for Tropical Technology. Samples were fractured in liquid nitrogen and sputter-coated with a thin platinum layer.

2.3.6. Surface wetting properties: Surface wettability was assessed by static contact-angle goniometry (DSA25, KRÜSS GmbH, Germany) under ambient conditions (25±2°C). Three probe liquids - distilled water, diiodomethane, and formamide - were used to determine the surface free energy (SFE) according to the Owens-Wendt-Rabel-Kaelble (OWRK) model. Samples were secured on glass slides, and a 10 µl microsyringe was used to gently dispense five droplets (5 µl each) of every liquid onto separate regions of the film before imaging. For each specimen, measurements were taken at three distinct locations and averaged. The total SFE and its dispersive and polar components were computed using ADVANCE software (KRÜSS GmbH, Germany).

2.3.7. Aging protocol: After initial testing (day 0), specimens were stored in a controlled chamber at 23±2°C, 50±5% RH and retrieved at 7, 28, and 56 days for tensile re-evaluation under identical conditions. Each timepoint included re-conditioning per ASTM D618 and ISO 291. Aging analysis focused on retention of σ_t and ε_b relative to day 0 (n=3).

2.3.8. X-ray diffractometry (XRD): Diffractograms were collected on a Bruker D8 ADVANCE (Germany) with Cu Kα radiation (λ=0.154 nm) at 40 kV/30 mA, scanning 2θ =10-70° at 2°/min (step 0.02°). Aged specimens were re-conditioned (ASTM D618/ISO 291) and measured under identical XRD settings. To qualitatively track short-range ordering upon storage, we computed a shoulder-to-halo index $I_{22.7}/I_{am}$, defined as the maximum intensity within 2θ=22.3-23.1° divided by a local amorphous baseline estimated

from a linear fit over 2θ=21.0-24.0°. Worked example and raw values are provided in Fig. S4 and Table S2 (SI).

2.3.9. Melt-flow index (MFI): MFI was measured according to ASTM D1238 Procedure A at 130°C with a 2.16 kg load using a 2.095×8 mm die. The reported value (g/10 min) is the average of n=3 replicates (±SD). To minimise thermal artefacts, the barrel was purged with N_2, residence time was kept short and identical across runs, and extrudate was visually inspected to rule out discoloration or char. The chosen temperature equals (or is below) the melt-processing setpoint used during compounding, so MFI reflects the processing-relevant flow state rather than thermal degradation.

Note on neat-DES thermal signatures. We did not perform DSC on the neat DES because their thermal transitions are highly water-sensitive and not readily comparable across laboratories without stringent water-activity control; instead, we anchor the analysis to composite-level metrics (DMA T_g/tan δ, processing rheology) that directly govern performance in use. Representative discussions of water-induced restructuring and property changes in DES are provided in the cited literature [11, 12].

3. Results and discussions

3.1. Processing behaviour and rheological response

The torque-time profiles and melt flow indices provide the first insight into the plasticisation efficiency of different DES formulations. By comparing Gly-rich, MEA-rich, and ternary compositions, the variations in peak torque, time to plateau, and flowability reveal how the nature of the hydrogen-bond donor influences starch chain mobility during melt processing.

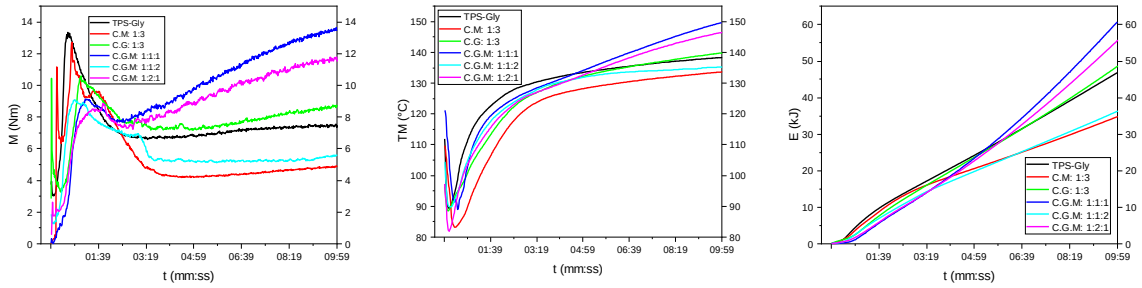

Fig. 1. Melt-processing response of cassava thermoplastic starch plasticised with glycerol and choline-chloride-based deep eutectic solvents.

Table 2A. Processing and rheological of samples: Steady torque at plateau (N·m), Terminal melt temperature (°C), melt-flow index (g/10 min). Mean ± SD (n=3).

Sample	Steady torque (N·m)	Terminal melt temperature (°C)	Melt-flow index (g/10 min)
TPS-Gly	7.4 ± 0.53	138.2 ± 7.8	1.02 ± 0.08
C.G: 1:3	8.7 ± 0.6	139.7 ± 11.3	1.01 ± 0.07
C.M: 1:3	4.8 ± 0.34	133.2 ± 7.7	2.15 ± 0.13
C.G.M: 1:1:1	13.5± 0.82	149.0 ± 9.2	0.87 ± 0.07
C.G.M: 1:1:2	5.5 ± 0.43	135.3 ± 9.1	2.45 ± 0.2
C.G.M: 1:2:1	11.6 ± 0.91	146.4 ± 8.5	0.92 ± 0.06

Table 2B. Thermoviscoelastic and mechanical properties samples: DMA T_g (°C), storage modulus E′ (MPa) (Mean ± SD, n = 3), tensile strength (MPa), elongation at break ε_b (%) (Mean ±SD, n=5).

Sample	Glass-transition temperature (°C)	E’ (MPa)	Tensile Strength (MPa)	Elongation at break (%)
TPS-Gly	72.4 ± 3.7	871.1 ±56.6	1.54 ± 0.1	169.9 ± 14.8
C.G: 1:3	31.9 ± 2.3	430.2 ± 27.5	0.97 ± 0.08	183.9 ± 15.3
C.M: 1:3	48.2 ± 2.9	639.5 ±46.0	2.27 ± 0.19	228.9 ±21.1
C.G.M: 1:1:1	49.7 ± 4.0	506.1 ± 39.5	3.33 ± 0.27	126.9 ± 14.2
C.G.M: 1:1:2	42.5 ± 2.6	875.8 ± 71.8	2.91 ± 0.27	195.1 ± 15.4
C.G.M: 1:2:1	57.9 ± 3.3	827.2 ± 51.3	2.31 ± 0.19	107.7 ± 9.6

The results in Fig. 1 and Table 2A show that, versus TPS-Gly (MFI≈1.02 g/10 min; torque≈7.4 N·m; final≈138 °C), ChCl:Gly (1:3) shows similar flow (1.01) but higher torque (≈8.7 N·m) and slightly higher final temperature (≈140°C). ChCl:MEA (1:3) markedly improves flow (MFI≈2.15) while lowering torque (≈4.8 N·m) and final temperature (≈133°C). The ternary ChCl:Gly:MEA (1:1:2) gives the best trade-off: MFI≈2.45, torque≈5.5 N·m, final≈135 °C, indicative of a low-viscosity yet cohesive melt.

In contrast, 1:1:1 (MFI≈0.87; torque≈13.5 N·m; final≈149°C) and 1:2:1 (MFI≈0.92; torque≈11.6 N·m; final≈146 °C) exhibit over-associated melts and narrower windows.

At fixed geometry and speed, steady torque grows with melt viscosity; conversely, MFI inversely scales with viscosity (and molecular weight), so high-MFI/low-torque pairs signify better flow at processing shear rates [13]. Glycerol supplies free volume (increased mobility), while MEA (-OH/-NH) forms directional H-bond/ion-pair junctions with ChCl and starch -OH, adding reversible network cohesion without over-penalising, consistent with DES literature and water-modulated amine-DES associations [14, 15]. Consequently, Gly-rich blends maximise mobility (high MFI) but risk low melt strength; increasing MEA raises transient associations and stabilises extensional flow. 1:1:2 balances these countervailing effects (high, stable MFI; moderate torque/temperature), whereas 1:1:1/1:2:1 enter an over-associated regime (high, torque, thermal dissipation). Importantly, lower torque and final melt temperature at comparable MFI reduce SME and widen the extrusion/injection window; ChCl:MEA (1:3) and especially ChCl:Gly:MEA (1:1:2) are thus expected to minimise energy input while preserving melt cohesiveness [16, 17].

3.2. FTIR spectroscopy: hydrogen-bonding interactions

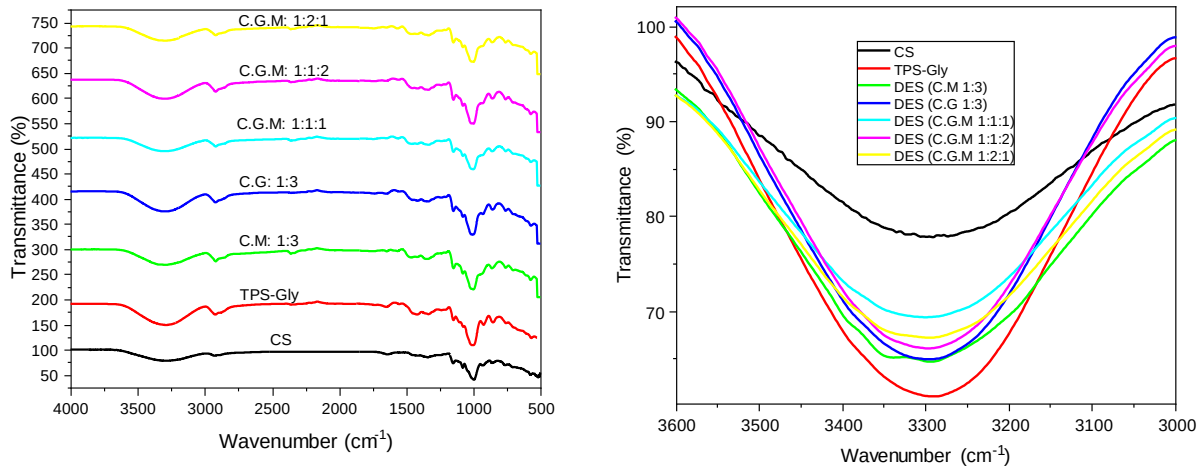

Fig. 2: ATR-FTIR spectra (4000–500 cm⁻¹) of TPS samples with different plasticisers. O-H envelope: red-shift and broadening diagnose networked H-bonding.

Fig. 2 compares the FTIR spectra of native cassava starch (CS), glycerol-plasticised cassava starch (TPS-Gly) and TPS plasticised with the ternary deep eutectic solvent (DES): ChCl:Gly:MEA at ratios of 1:0:3, 1:3:1, 1:1:1, 1:1:2, 1:2:1. In all plasticised samples, the broad O-H stretching vibrations (in the 3600-3000 cm^{-1} wavenumber region) shifted to lower wavenumbers and became broader compared to CS. The red-shift and broadening

were most pronounced for DES, especially the MEA-rich sample, consistent with more effective disruption of starch-starch interactions compared to glycerol. This behaviour may be promoted by the bifunctional -OH-NH_2 groups of MEA, which provide both donor and acceptor sites for hydrogen bonding with starch hydroxyls [18]. The ν(N-H) (≈3350-3300 cm^{-1}) and δ(NH_2) (~1600 cm^{-1}) assignments are in line with recent MEA infrared studies [19]. Together with the HBA character of ChCl, these signatures point to dual-mode plasticisation: glycerol predominantly increases free volume and chain mobility, while MEA furnishes directional H-bond/ion-pair associations with ChCl and starch hydroxyl groups (AGU-OH), yielding a more cohesive yet processable matrix. This spectroscopic picture aligns with processing/DMA trends (enhanced flow, moderated T_g decrease) and rationalises the broader processing window and improved anti-retrogradation of the ternary DES relative to TPS-Gly.

In the fingerprint region (≈1200-900 cm^{-1}), all DES-plasticised TPS displayed subtle (few-cm^{-1}) red-shifts and intensity redistribution within the C-O-C/C-O stretching envelope (≈1155-995 cm^{-1}). Relative to TPS-Gly, MEA-containing and the 1:1:2 ternary systems showed a qualitatively lower 1047/1022 band ratio, together with a modest enhancement near ≈995-1010 cm^{-1}, consistent with reduced short-range order and higher amorphicity. These trends are coherent with the O–H red-shift/broadening discussed above (Fig. 2).

3.3. X-Ray Diffraction (XRD) Patterns

The XRD patterns (Fig. S3) reveal the degree of structural ordering introduced by different DES systems. Immediately after melt-processing, all DES-plasticised TPS exhibit a dominant amorphous halo at ~19-20° (2θ) with marked attenuation of native A-type reflections near ~15°, 17-18°, and 22-23°, indicating extensive amorphisation. This response-loss or attenuation of A-type peaks and dominance of an ~20° halo - matches established assignments of starch polymorphs and typical TPS behaviour following plasticisation and shear/thermal treatment [20].

Across formulations, the Gly-rich systems retained the most order (discernible shoulders near ~17-18° and ~23°), whereas MEA-containing DES (binary ChCl:MEA and the ternary ChCl:Gly:MEA) produced more featureless halos with lower relative peak intensities-consistent with deeper disruption of inter- and intramolecular packing. Mechanistically, polyol-dominant plasticisation (Gly) increases free volume and segmental

mobility, which facilitates helix re-association upon cooling, while MEA-containing DES introduce stronger, directional H-bond/ion-pair interactions that better "lock" chains in disordered states during quench, delaying recrystallisation. These trends align with contemporary reports that DESs (particularly amide/amine-bearing systems) penetrate/crack ordered lamellae and suppress immediate recrystallisation in starch matrices [10, 21].

Under the melt-processing conditions applied (short residence, low water), ChCl:MEA acts as a plasticiser/destructuring medium rather than a molecular solvent for starch; the XRD amorphisation and FTIR O-H broadening therefore reflect destructuration/gelatinisation, not full dissolution.

3.4. Thermal-viscoelastic properties (DMA)

Dynamic mechanical analysis (DMA) in single-cantilever mode (1 Hz, from -40 to 120°C, within the LVR) resolves the temperature-dependent storage modulus (E′) and the main relaxation (tan δ) associated with starch-chain segmental mobility. T_g is taken at the tan δ maximum.

Interpretive note: In polymer-plasticiser systems, the relevant glass transition for mechanics and processing is that of the polymer-rich (starch-rich) phase, which we quantify by DMA, rather than the T_g/T_m of the neat plasticiser. This view is consistent with mixing-rule descriptions (e.g., Gordon-Taylor/Fox) widely applied to plasticised amorphous solids [12, 13]. Together with the pronounced water-sensitivity of neat-DES thermal signatures reported in the literature, which limits cross-laboratory comparability without rigorous water control, neat-DES DSC would add limited interpretive value here. Accordingly, our discussion of mobility relies on DMA T_g/tan δ and processing rheology (torque/MFI), which directly govern performance [23, 24].

The analysis results (Fig. S1 and Table 2B) show that, replacing neat glycerol with choline-based DES depresses T_g, with the magnitude governed by the Gly/MEA balance: ChCl:Gly (1:3) gives the lowest T_g (≈32°C; ΔT_g≈-40°C vs TPS-Gly≈72°C), whereas ChCl:MEA (1:3) partially recovers T_g to≈48°C (ΔT_g≈ -24°C). Ternary systems are non-monotonic: 1:1:2≈42.5°C, 1:1:1≈49.7°C, 1:2:1≈57.9°C - indicating a tuneable mobility-association balance.

At sub-T_g temperatures, TPS-Gly exhibits the highest E′ plateau (≈871 MPa), while DES-plasticised TPS show lower but composition-dependent E′ (≈430-830 MPa). Within

the ternaries, 1:1:2 maintains higher E′ than ChCl:Gly, consistent with MEA-reinforced, reversible H-bond/ion-pair junctions that preserve melt cohesion without forfeiting softness. The Gly-rich DES (e.g., ChCl:Gly) maximise free-volume creation and thus shift T_g downward more strongly, whereas MEA-containing systems (e.g., ChCl:MEA or ternaries containing MEA) partially recover T_g due to additional directional -OH/-NH hydrogen-bond/ion-pair junctions that "anchor" segments and moderate mobility. These trends align with the established roles of DES components in TPS-polyols acting as efficient plasticisers and amine-containing HBDs introducing stronger associations [8, 16, 22]. The specific influence of MEA-based DES and of water traces on their supramolecular structure further supports this dual-mode picture [14].

Collectively, the DMA trends support a dual-mode plasticisation: glycerol predominantly supplies free volume (strong T_g depression, higher tan δ), whereas MEA introduces directional associations with ChCl and starch -OH that modestly raise T_g and damp tan δ. These outcomes align with torque/MFI (MEA-containing DES combine good flow with adequate melt strength) and FTIR signatures (O-H red-shift; emergent ν(N-H)/δ(NH_2)) [8, 21, 22]. Notably, the 1:1:2 ternary offers the most favourable trade-off between mobility and supramolecular association.

In this work, free-volume changes are inferred rather than assumed, by combining multiple measured proxies with well-established theoretical frameworks. First, the T_g depression and concomitant reduction of storage modulus E′ (DMA) reflect increased segmental mobility; together with the tan δ peak shift and broadening, these responses are consistent with a larger fractional free volume and a broader distribution of local environments. Second, the lower melt viscosity/processing torque (i.e., higher MFI under matched conditions) conforms to the Doolittle/Cohen-Turnbull view that viscosity decreases exponentially with increasing free volume. Third, FTIR evidence - O-H red-shift/broadening and intensity redistribution within the 1155–995 cm^{-1} envelope with a qualitatively lower 1047/1022 ratio - indicates disruption of short-range order in the AGU network, cohering with added interstitial volume. In aggregate, these signatures align with WLF and Gordon-Taylor/Kelley-Bueche relations for plasticised amorphous matrices, and they underpin the glycerol<MEA<DES(ChCl:MEA) ranking observed here. We therefore attribute the stronger plasticisation by DES to cooperative hydrogen-bonding plus ion-pair interactions that both weaken native starch-starch cohesion and act as effective spacers,

increasing the accessible free volume without invoking any unmeasured assumptions.

3.5. Morphology and mechanical performance

SEM imaging coupled with tensile testing was conducted to assess how DES composition affects microstructural homogeneity and macroscopic mechanical behaviour. Differences in domain size, fracture morphology, and stress-strain responses illustrate the trade-off between elongation and tensile strength in Gly- and MEA-dominated systems.

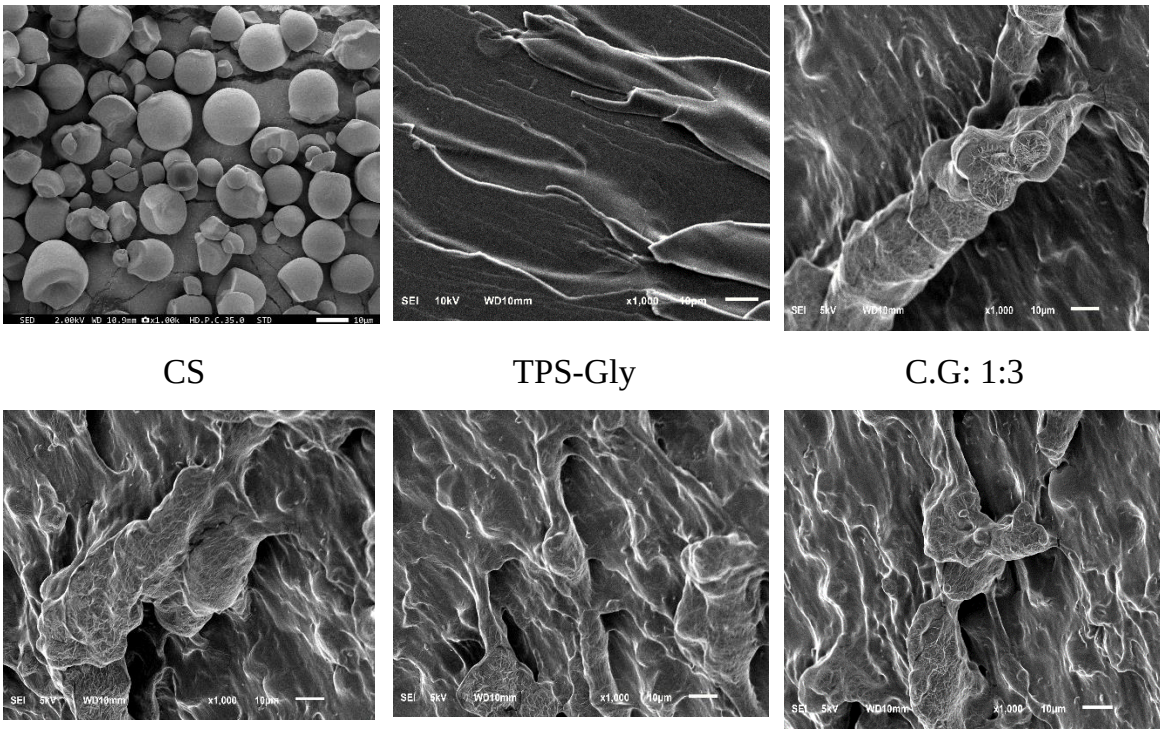

Fig. 3. SEM image of CS and TPS samples.

Cryo-fractured specimens were sputter-coated with Pt and imaged by SEM (SM-6510LV). Fig. 3 displays the fracture surfaces for TPS-Gly, ChCl:Gly (1:3), ChCl:MEA (1:3), and the ternaries ChCl:Gly:MEA (1:1:1; 1:1:2; 1:2:1) [23]. MEA-based DES (ChCl:MEA 1:3) yields smoother, more homogeneous planes with fewer voids, indicating a higher density of reversible -OH/-NH hydrogen-bond/ion-pair junctions between MEA, ChCl, and starch, aligning with moderated T_g and partial strength recovery reported for amine-containing DES [24]. Ternaries (ChCl:Gly:MEA) exhibit a composition-dependent balance: 1:1:1 shows flatter, feature-poor facets (over-association); 1:2:1 presents locally rougher regions and occasional voids (insufficient junction density); 1:1:2 displays the most uniform, defect-sparse surface, evidencing efficient stress transfer without brittle cleavage. Collectively, the micrographs support dual-mode plasticisation: glycerol

promotes mobility and cavitation, whereas MEA introduces reversible junctions that homogenise the microstructure; 1:1:2 best balances these effects, mirroring the strength–elongation trade-off in this series [25].

Tensile properties

Mechanical properties (Fig. S4; Table 2). Under identical conditions (ASTM-type specimens; n=5, mean ± SD), DES composition dictates the strength–ductility envelope via dual-mode plasticisation. Glycerol-dominated systems prioritise mobility: TPS-Gly (TS=1.54±0.10 MPa; ε_b=169.9±14.8%) and ChCl:Gly (1:3) (TS=0.97±0.08 MPa; ε_b=183.9±15.3%) show ductile flow at low stress. In contrast, ChCl:MEA (1:3) simultaneously increases strength and extensibility (TS=2.27±0.19 MPa; ε_b=228.9±21.1%), consistent with reversible -OH/-NH H-bond/ion-pair junctions that restore load bearing without over-constraining chains. The ternaries map a tuneable compromise: 1:1:1 maximises cohesion (TS=3.33±0.27 MPa; ε_b=126.9±14.2%), 1:2:1 limits extensibility (TS=2.31±0.19 MPa; ε_b=107.7±9.6%), whereas 1:1:2 offers the best balance (TS=2.91±0.27 MPa; ε_b=195.1±15.4%). These trends align with SEM (rough, voided surfaces in Gly-rich vs. uniform, defect-sparse in MEA-containing/1:1:2) and support a composition-structure-property framework: glycerol supplies free volume; MEA provides supramolecular junctions; 1:1:2 balances both to deliver high strength at sustained ductility. Within the explored composition window, the strength of the free-volume–driven plasticisation follows glycerol<MEA DES(ChCl:MEA), in line with the progressively stronger bond-disrupting/spacing effects expected from hydroxyl-only (glycerol), hydroxyl-plus-amine (MEA), and amine-ionic (ChCl:MEA DES) interactions.

3.6. Wettability and Surface Free Energy by Contact Angle (OWRK)

Table 3. Surface free energy components and contact angle of TPS samples (mean ±SD, n=3).

Samples	Water (θ, °)	Formamide (θ, °)	Diiodomethane (θ, °)	Dispersive part, γ^d, mN.m^{-1}	Polar part, γ^p, mN.m^{-1}	Surface Free Energy, γ, mN.m^{-1}
TPS-Gly	42.1 ± 3.4	36.3 ± 3.2	28.7 ± 2.5	32.2 ± 2.9	22.5 ± 2.0	54.7 ± 4.9
C.G: 1:3	45.0 ± 3.8	39.5 ± 3.3	30.5 ± 2.6	31.5 ± 2.6	20.0 ± 1.8	51.5 ± 4.1
C.M: 1:3	71.5 ± 6.8	63.0 ± 5.5	44.0 ± 3.8	31.4 ± 2.4	7.4 ± 0.6	38.8 ± 3.0

C.G.M: 1:1:1	56.0 ± 4.6	50.0 ± 4.1	38.0 ± 3.2	30.6 ± 2.3	14.8 ± 1.2	45.4 ± 3.5
C.G.M: 1:1:2	61.0 ± 5.0	55.0 ± 4.4	40.0 ± 3.3	30.0 ± 2.2	12.0 ± 1.1	42.0 ± 3.0
C.G.M: 1:2:1	50.0 ± 4.2	44.5 ± 3.8	34.0 ± 2.9	31.0 ± 2.4	17.5 ± 1.5	48.5 ± 3.8

The OWRK analysis (Table 3) shows that replacing glycerol with MEA lowers surface polarity while γd remains ≈30–32 mN·m⁻¹; diiodomethane angles change little, confirming polarity-controlled wettability. Versus TPS–Gly (θ_{water} = 42.1 ± 3.4°, γ^d = 32.2 ± 2.9, γ^p = 22.5 ± 2.0, γ = 54.7 ± 4.9 mN·m⁻¹), ChCl:Gly (1:3) shows a small γ drop (γ = 51.5 ± 4.1) from modest γ^p loss (20.0 ± 1.8). ChCl:MEA (1:3) yields much higher contact angles (θwater = 71.5 ± 6.8°; $\theta_{formamide}$ = 63.0 ± 5.5°) and the lowest γ (38.8 ± 3.0) due to a sharp γ^p decline (7.4 ± 0.6) at nearly unchanged γ^d (31.4 ± 2.4). Ternaries interpolate non-monotonically: 1:2:1 (48.5 ± 3.8) > 1:1:1 (45.4 ± 3.5) > 1:1:2 (42.0 ± 3.0 mN·m⁻¹), tracking a monotonic γ^p decrease (17.5 → 12.0 mN·m⁻¹) at near-constant γ^d (30–31). Diiodomethane angles change little, confirming polarity, not dispersion, governs wettability. Methodologically, water+diiodomethane +formamide enable Owens–Wendt–Rabel–Kaelble resolution of γ into γ^d and γ^p with an improves robustness [26, 27]. The MEA-containing DES reorient/engage surface –OH via reversible –OH/–NH H-bond/ion-pair junctions, reducing accessible polar groups at the air/solid interface; glycerol-rich surfaces retain higher γ^p. For applications, ChCl:MEA (1:3) and 1:1:2 offer lower γ and higher water contact angle (moisture resistance), whereas glycerol-dominant formulations favour printability/adhesion. Notably, 1:1:2 couples moderate γ (42.0 mN·m⁻¹) with balanced mechanics, marking a practical design window [28].

Although barrier properties (WVTR/OTR) were not measured here, lower γ and γ^p together with higher θ_{water} for MEA-containing systems qualitatively suggest reduced water uptake and potentially lower WVTR relative to TPS–Gly. Nevertheless, gas transport also depends on bulk free volume and crystallinity; our XRD indicates substantial amorphisation in DES systems, which may increase OTR. We therefore anticipate moderate improvement in water-vapor resistance for 1:1:2 and a neutral-to-mixed effect on oxygen transport—an aspect prioritised for future validation.

3.7. Retrogradation

Table 4. Summary of mechanical properties and % change of TPS samples stored at 0 and 56 days.

Samples	Storage time, days: 0		Storage time, days: 56			
	TS (MPa)	***ε_b (%)***	***TS (MPa)***	***ε_b (%)***	***ΔTS vs 0 (%)***	***$\Delta\varepsilon_b$ vs 0 (%)***
TPS-Gly	1.54 ± 0.1	169.9 ± 14.8	0.79 ± 0.07	85.49 ± 8.6	-48.7±3.5	−49.7±5.3
C.G: 1:3	0.97 ± 0.08	183.9 ± 15.3	0.90 ± 0.08	88.0 ± 9.0	−7.2±0.6	−52.2±6.1
C.M: 1:3	2.27 ± 0.19	228.9 ±21.1	2.0 ± 0.1	149.49 ± 10.2	−11.9±1.0	−34.7±4.3
C.G.M: 1:1:1	3.33 ± 0.27	126.9 ± 14.2	3.02 ± 0.27	88.0 ± 10.0	-9.2±0.7	−30.7±3.1
C.G.M: 1:1:2	2.91 ± 0.27	195.1 ± 15.4	2.7 ± 0.24	162.0 ± 12.0	-7.2±0.7	−17.0±1.6
C.G.M: 1:2:1	2.31 ± 0.19	107.7 ± 9.6	2.01 ± 0.18	84.0 ± 8.0	−8.8±0.9	−22.0±2.1

We focus aging assessments on mechanical endpoints because they provide a sensitive, application-level integration of microstructural changes under standardised humidity. These results are interpreted on top of the baseline structure–dynamics fingerprint established immediately after processing (XRD amorphisation; FTIR O–H red-shift/broadening and fingerprint-region redistribution; DMA T_g/E′ depression). Under 23 ± 2 °C and 50 ± 5% RH re-conditioning prior to each time point, the systematic loss of ductility at near-constant tensile strength is a classical signature of physical retrogradation and reflects performance-relevant consequences of structural re-organisation.

Accordingly, physical retrogradation is inferred from the systematic loss of ductility at near-constant tensile strength under standardised humidity (Table S1 and Table 4), together with composition-dependent T_g/E′ responses (Fig. S2). Baseline diffractograms (Fig. S3) of freshly processed samples confirm extensive amorphisation (with Gly-rich systems retaining the most residual order), which coheres with the larger ε_b loss upon storage.

Across all formulations, storage at 23 ± 2 °C and 50 ± 5 % RH led to a monotonic loss in ductility while TS remained comparatively stable - classical signatures of physical retrogradation (Table S1 and Table 4) - hallmarks of physical retrogradation. Quantitatively, TPS–Gly deteriorates most (TS 1.55→0.79 MPa, −48.7%; ε_b 170.3→85.5%, −49.7%). The ChCl:Gly (1:3) retains TS (0.97→0.90 MPa, −7.2%) but still loses ε_b sharply (183.9→88.0%, −52.2%). The ChCl:MEA (1:3) ages more gently (TS 2.27→2.00 MPa, −11.9%; ε_b 228.9→149.5%, −34.7%). Among ternaries, the C.G.M 1:1:2 performs best (TS 2.91→2.70 MPa, −7.2%; ε_b 195.1→162.0%, −17.0%), whereas the C.G.M 1:1:1 favours strength at the cost of extensibility (ε_b −30.7%) and the C.G.M 1:2:1

shows a moderate ε_b drop (−22.0%). ε_b-retention ranking: 1:1:2 > 1:2:1 > 1:1:1 > ChCl:MEA (1:3) » ChCl:Gly (1:3) ≈ TPS–Gly. These trends are consistent with the aged-XRD fingerprints (Fig. S4; Table S2). TPS–Gly and ChCl:Gly (1:3) develop weak shoulders at ~17–18° and 22–23°, captured by a marked rise of the intensity index $I_{22.7}/I_{am}$ from 0.053 → 0.369 (TPS–Gly) and 0.055 → 0.737 (ChCl:Gly 1:3). By contrast, ChCl:MEA (1:3) shows only modest growth (0.092 → 0.262) and the ternary ChCl:Gly:MEA (1:1:2) exhibits minimal change (0.079 → 0.130) without discrete new peaks above the noise floor; only halo narrowing is observed. These XRD trends mirror mechanical retention: ε_b decreases strongly for TPS–Gly (170.3 → 85.5 %) and ChCl:Gly 1:3 (183.9 → 88.0 %), but is better preserved for ChCl:MEA 1:3 (184.1 → 149.5 %) and especially for the ternary 1:1:2 (195.1 → 162.0 %). Together, the suppressed peak growth and higher ε_b retention in MEA-containing systems support the view that MEA-enabled H-bond/ion-pair junctions reduce water-assisted chain rearrangement and thus restrain retrogradation.

Polyol-rich networks generate free volume and mobile H-bond bridges—boosting initial εb but facilitating moisture uptake, chain rearrangement, and recrystallisation, hence embrittlement (classically $\varepsilon_b\downarrow$ with modest TS change) [7, 29, 30]. Plasticiser migration can further stiffen the amorphous phase [31]. In contrast, amine/amide plasticisers (e.g., MEA, urea) form stronger, more specific H-bond/ion-pair junctions that suppress retrogradation and better preserve ε_b over time; dense HB networks in DES can even impart long-term resistance [29, 30]. Consistently, higher water contact angle and lower OWRK γ^p correlate with slower aging, explaining the superior retention of MEA-containing and especially 1:1:2 systems.

Across formulations, reductions in the polar component of surface free energy (γ^p) correlate with improved ε_b-retention during 56-day storage. Replacing glycerol with MEA-containing DES lowers γ^p while maintaining γ^d; this coincides with markedly smaller ductility loss (e.g., $\Delta\varepsilon_b \approx -17\%$ for 1:1:2 vs $\approx -50\%$ for TPS–Gly). We ascribe this trend to reduced availability of accessible surface –OH groups (lower γ^p), which diminishes moisture sorption and water-mediated chain rearrangements that typically accelerate retrogradation. Thus, γ^p serves as a convenient proxy for the propensity to undergo water-facilitated secondary crystallisation.

Plasticiser migration was not quantified; nevertheless, the combination of a relatively stable TS with a monotonic ε_b decrease, the initial amorphisation (XRD), and the wettability trends indicates that retrogradation is the primary driver of embrittlement under our storage conditions, although minor migration, particularly in glycerol-rich systems, cannot be entirely ruled out.

While humidity-controlled, time-resolved XRD/DMTA can map crystallite-regrowth kinetics, under the present standardised conditioning they would serve as confirmatory probes; the convergence of baseline XRD/FTIR/DMA with the aged mechanical response already substantiates our conclusions. Such measurements are therefore deferred to future work.

4. Conclusion

This study maps the composition–structure–property space of cassava TPS plasticised with choline-based DES at 25 wt% (ChCl:Gly, ChCl:MEA, and ChCl:Gly:MEA) and evidences a dual-mode plasticisation: glycerol supplies free volume, whereas MEA introduces reversible –OH/–NH hydrogen-bond/ion-pair junctions. Convergent data from mixing/MFI/SME, FTIR-ATR, DMA, SEM, OWRK, and 56-day aging show that mobility and supramolecular association can be co-tuned by DES composition to achieve processability without forfeiting cohesion. Quantitatively, Gly-only/Gly-rich systems enhance flow but depress cohesion; MEA-based DES lower torque and melt temperature, increase MFI, and simultaneously strengthen the stress–strain response. The ternary 1:1:2 delivers the best balance: MFI ≈ 2.45 g/10 min, torque ≈ 5.5 N·m, TS ≈ 2.91 MPa, ε_b ≈ 195%, and the lowest 56-day ductility loss ($\Delta\varepsilon_b$ ≈ −17%), far outperforming glycerol controls (≈ −50%). Mechanistic signatures (O–H red-shift/broadening with emergent ν(N–H)/$\delta(NH_2)$; moderated T_g with sustained E'; $\gamma^p\downarrow$ at γ^d ≈ 30–32 mN·m^{-1}; increased amorphisation/delayed recrystallisation) support that MEA-enabled junctions counterbalance Gly-induced free volume, stabilising the amorphous phase and decoupling viscosity reduction from melt-strength loss. Mechanistically, glycerol-dominant DES increase free volume and chain mobility, whereas MEA-containing DES introduce reversible H-bond/ion-pair junctions; tuning their ratio yields viscosity reduction without loss of melt strength and improves aging resistance. These principles should extend to other HBD/HBA pairs beyond ChCl:Gly:MEA. Future work

should quantify barrier properties (WVTR/OTR), assess plasticiser migration across humidity/temperature, and validate the map across processing platforms.

Although plasticiser migration was not quantified, the weight of evidence—stable TS alongside a monotonic decrease in ε_b, initial amorphisation (XRD), and lower polar surface-energy, supports retrogradation as the primary cause of aging-induced embrittlement under the storage conditions employed here. Beyond MEA, the dual-mode plasticisation concept advanced in this work (polyol-driven free volume plus amine/amide-mediated H-bond/ion-pair junctions with ChCl) is expected to extend to other amine-containing DES with composition-dependent trade-offs between stiffness retention and mobility. Collectively, the composition–structure–property map clarifies how HBA–HBD balance governs mobility versus supramolecular association in TPS; these relationships are general and not tied to a specific processing line..

Mechanistic signatures: While DSC gelatinisation and granule-scale microscopy are valuable confirmatory tools, the present XRD/FTIR/DMA/SEM set already captures the structural consequences (loss of A-type order, increased amorphicity and segmental mobility) that DSC/microscopy would diagnose; further calorimetry/imaging is therefore deferred to future work.

Limitations

While we provide literature context for neat-DES thermal behaviour, our conclusions do not rely on any absolute T_g/T_m of the neat DES; they rest on composite-level DMA and rheology, which are the controlling parameters for TPS performance.

CRediT author statement

Chien Van Nguyen, Mai Thi Pham: Conceptualisation, Literature Review, Data Analysis, Writing - Original Draft Preparation; Phuong Thi Hoang: Supervision, Reviewing And Editing.

ACKNOWLEDGEMENTS

The current research received funding from the Vietnam Academy of Science and Technology under grant number TĐNSH0.01/22-24.

COMPETING INTEREST

The authors declare that there is no conflict of interest regarding the publication of this article.

REFERENCES

1. Averous, L., (2004), "Biodegradable multiphase systems based on plasticised starch: a review." *Journal of Macromolecular Science, Part C: Polymer Reviews*. **44**(3): p. 231-274

2. Ibrahim, M., et al., (2019), "Physical, thermal, morphological, and tensile properties of cornstarch-based films as affected by different plasticisers." *International journal of food properties*. **22**(1): p. 925-941

3. Lourdin, D., et al., (1997), "Influence of equilibrium relative humidity and plasticiser concentration on the water content and glass transition of starch materials." *Polymer*. **38**(21): p. 5401-5406

4. Mathew, A.P. and A. Dufresne, (2002), "Plasticised waxy maize starch: effect of polyols and relative humidity on material properties." *Biomacromolecules*. **3**(5): p. 1101-1108

5. Paluch, M., et al., (2022), "Structural and thermal properties of starch plasticised with glycerol/urea mixture." *Journal of Polymers and the Environment*. **30**(2): p. 728-740

6. Ma, X., J. Yu, and J.F. Kennedy, (2005), "Studies on the properties of natural fibers-reinforced thermoplastic starch composites." *Carbohydrate Polymers*. **62**(1): p. 19-24

7. Ma, X.F., J. Yu, and J. Wan, (2006), "Urea and ethanolamine as a mixed plasticiser for thermoplastic starch." *Carbohydrate polymers*. **64**(2): p. 267-273

8. Zdanowicz, M., K. Wilpiszewska, and T. Spychaj, (2018), "Deep eutectic solvents for polysaccharides processing. A review." *Carbohydrate polymers*. **200**: p. 361-380

9. Zdanowicz, M., et al., (2022), "Thermoplastic starch/ternary deep eutectic solvent/lignin materials: study of physicochemical properties and fire behaviour." *ACS Sustainable Chemistry & Engineering*. **10**(14): p. 4579-4587

10. Skowrońska, D. and K. Wilpiszewska, (2022), "Deep eutectic solvents for starch treatment." *Polymers*. **14**(2): p. 220

11. Hancock, B.C. and G. Zografi, (1994), "The relationship between the glass transition temperature and the water content of amorphous pharmaceutical solids." *Pharmaceutical research*. **11**(4): p. 471-477

12. Chaudhary, D.S., B.P. Adhikari, and S. Kasapis, (2011), "Glass-transition behaviour of plasticised starch biopolymer system–A modified Gordon–Taylor approach." *Food Hydrocolloids*. **25**(1): p. 114-121

13. Cheng, B., et al., (2001), "Evaluation of rheological parameters of polymer melts in torque rheometers." *Polymer Testing*. **20**(7): p. 811-818

14. Li, M., et al., (2022), "Effect of water on amine-based deep eutectic solvents (choline chloride+ monoethanolamine): Structure and physicochemical properties." *Journal of Environmental Chemical Engineering*. **10**(1): p. 106952

15. Faraone, A., et al., (2018), "Glycerol hydrogen-bonding network dominates structure and collective dynamics in a deep eutectic solvent." *The Journal of Physical Chemistry B*. **122**(3): p. 1261-1267

16. Zdanowicz, M. and K. Sałasińska, (2023), "Characterisation of thermoplastic starch plasticised with ternary urea-polyols deep eutectic solvent with two selected fillers: microcrystalline cellulose and montmorillonite." *Polymers*. **15**(4): p. 972

17. Banerjee, R. and S.S. Ray, (2023), "Role of rheology in morphology development and advanced processing of thermoplastic polymer materials: a review." *ACS omega*. **8**(31): p. 27969-28001

18. Gómez-López, R.A., et al., (2023), "Co-plasticisation of starch with glycerol and isosorbide: effect on retrogradation in thermo-plastic cassava starch films." *Polymers*. **15**(9): p. 2104

19. McWilliams, L.E., et al., (2015), "A means to an interface: investigating monoethanolamine behaviour at an aqueous surface." *Physical Chemistry Chemical Physics*. **17**(33): p. 21458-21469

20. Chamorro, A.F., M. Palencia, and T.A. Lerma, (2025), "Physicochemical Characterisation and Properties of Cassava Starch: A Review." *Polymers*. **17**(12): p. 1663

21. Zdanowicz, M., (2021), "Deep eutectic solvents based on urea, polyols and sugars for starch treatment." *International Journal of Biological Macromolecules*. **176**: p. 387-393

22. Zdanowicz, M., (2020), "Starch treatment with deep eutectic solvents, ionic liquids and glycerol. A comparative study." *Carbohydrate polymers*. **229**: p. 115574

23. Florez, J.P., M. Fazeli, and R.A. Simão, (2019), "Preparation and characterisation of thermoplastic starch composite reinforced by plasma-treated poly

(hydroxybutyrate) PHB." *International journal of biological macromolecules*. **123**: p. 609-621

24. Staker, J., et al., (2024), "Influence of choline chloride/urea and glycerol plasticisers on the mechanical properties of thermoplastic starch plastics." *Polymers*. **16**(6): p. 751

25. Weerasinghe, U.A., et al., (2024), "Deep eutectic solvents towards green polymeric materials." *Green Chemistry*. **26**(15): p. 8497-8527

26. Owens, D.K. and R. Wendt, (1969), "Estimation of the surface free energy of polymers." *Journal of applied polymer science*. **13**(8): p. 1741-1747

27. Kaelble, D., (1970), "Dispersion-polar surface tension properties of organic solids." *The Journal of Adhesion*. **2**(2): p. 66-81

28. Zdanowicz, M., (2023), "Influence of Urea Content in Deep Eutectic Solvents on Thermoplastic Starch Films' Properties." *Applied Sciences*. **13**(3): p. 1383

29. Surendren, A., et al., (2022), "A review of biodegradable thermoplastic starches, their blends and composites: recent developments and opportunities for single-use plastic packaging alternatives." *Green Chemistry*. **24**(22): p. 8606-8636

30. Huang, M., J. Yu, and X. Ma, (2005), "Ethanolamine as a novel plasticiser for thermoplastic starch." *Polymer degradation and stability*. **90**(3): p. 501-507

31. Esmaeili, M., et al., (2019), "Poly (lactic acid)/plasticized thermoplastic starch blend: Effect of plasticiser migration on rheological and mechanical properties." *Polymers for Advanced Technologies*. **30**(4): p. 839-851.